Analytica Chimica Acta 1105 (2020) 82–86

Contents lists available at ScienceDirect

Analytica Chimica Acta

journal homepage: www.elsevier.com/locate/aca

Electrochemical sensing of pancreatic cancer miR-1290 based on yeast-templated mesoporous TiO_2 modified electrodes

Xuping Wang [a], Jingjie Cui [a, *], Shaowei Chen [b], Yong Yang [a], Li Gao [c, **], Qingfang He [d]

[a] School of Automation, Hangzhou Dianzi University, Hangzhou, 310018, China
[b] Department of Chemistry and Biochemistry, University of California, 1156 High Street, Santa Cruz, CA, 95064, USA
[c] Institute of Life Sciences, Jiangsu University, 301 Xuefu Road, Zhenjiang, 212013, China
[d] Zhejiang Provincial Center for Disease Prevention and Control, Hangzhou, 310051, China

HIGHLIGHTS

- The yeast mesoporous TiO_2 was assembled by biomimetic synthesis.
- The yeast mesoporous TiO_2 showed excellent electrocatalytic performance.
- The yeast mesoporous TiO_2 could detect pancreatic cancer miRNAs with single-nucleotide discrimination.

GRAPHICAL ABSTRACT

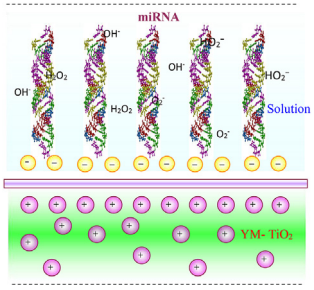

ARTICLE INFO

Article history:
Received 29 September 2019
Received in revised form
11 January 2020
Accepted 14 January 2020
Available online 20 January 2020

Keywords:
Yeast
Mesoporous Titania
miRNA
Cancer
Electrochemical sensing detection

ABSTRACT

Electrochemical sensing is an effective, low-cost technology for cancer detection. In this study, mesoporous TiO_2 was prepared via biomimetic synthesis based on yeast cell templates, and used to prepare a modified electrode for the sensitive detection of pancreatic cancer miR-1290. The structure and the morphology of the TiO_2 were characterized by X-ray diffraction (XRD), N_2 adsorption-desorption isotherm (NADI), Atomic force microscopy (AFM), and electron probe microanalysis (EPMA). As a sensing active material, the yeast-templated mesoporous TiO_2 could detect pancreatic cancer miRNAs with single-nucleotide discrimination. The sample prepared by calcination at 400 °C showed the best electrochemical sensing activity. Moreover, compared with the blank electrode, the yeast mesoporous TiO_2 sensing electrode could oxidize the pancreatic cancer microRNAs at a lower potential, which minimized the interference from oxygen evolution reaction at high potentials.

1. Introduction

Cancer has become a severe disease that plagues human health. According to statistics from the World Health Organization, about 8.8 million people die of cancer every year in the world [1,2]. However, if a patient can receive an early diagnosis, the mortality rate will be significantly reduced [3]. Therefore, early diagnosis of cancer, in particular, non-destructive and non-invasive detection, is crucial in the diagnosis and treatment of cancer.

MicroRNAs (miRNAs) are a class of highly conserved non-coding small RNAs of 18–25 nucleotides in length, which can be widely found in plants and animals [4]. miRNA is involved in many kinds of biological processes in tumorigenesis and development by regulating the cell cycle, apoptosis, cell migration, and angiogenesis; and plays key roles in early detection of cancer. Changes in miRNA expression levels can serve as fingerprints and provide information

* Corresponding author.
** Corresponding author.
E-mail addresses: cui@hdu.edu.cn (J. Cui), gaoli@ujs.edu.cn (L. Gao).

https://doi.org/10.1016/j.aca.2020.01.030
0003-2670/

about cancer status and progression [5,6]. miR-1290 is a highly sensitive and specific biomarker for the diagnosis and prediction of patients with pancreatic cancer [7]. Li et al. [8] detected the expression profile of miRNA in 735 pancreatic cancer patients and normal control serum, and found that miR-1290 was up-regulated in peripheral blood of patients with pancreatic cancer, which helped distinguish patients with early pancreatic cancer.

The traditional detection technique of Northern blotting and in situ hybridization is laborious and lacks sensitivity. New technologies, such as chip technology and quantitative polymerase chain reaction (qPCR), while powerful, are still limited to central laboratories due to their complexity. Therefore, it is urgent to develop facile technologies to detect miRNA levels.

Electrochemistry is widely used in the fields of life science, biomedicine, and so on, because of its outstanding advantages, such as good selectivity, high sensitivity, and rapid, economical, and continuous real-time monitoring [9]. The performance of electrochemical sensor depends on the activity of the sensing electrode materials [10]. The research of electrocatalytic active materials has been a crucial subject in the development of electrochemical sensors. Moreover, the electrochemical sensing process in aqueous solution often involves an oxygen reduction reaction, so the electrode materials should ideally exhibit an excellent electrocatalytic activity towards oxygen reduction [11]. Notably, the mass transfer capacity of oxygen is poor in the liquid phase [12]. The solubility (about 10^{-4} mol/L) and diffusion coefficient (10^{-9} m^2/s) of oxygen in electrolyte solution are small [13,14]. In order to improve the performance of the sensing electrode, we should decrease the boundary layer thickness of the liquid mass transfer as much as possible while increasing the actual surface area of the electrode. Because of their unique porosity, porous materials have many physical and chemical properties, such as high specific surface area, high porosity, and high permeability, which are conducive to the development of high-efficiency sensing electrodes. Titanium dioxide (TiO_2) is a multifunctional material with excellent chemical, electronic, photoelectric and photovoltaic properties [15,16]. More importantly, as an excellent sensing material, TiO_2 film has been applied to the sensing of water vapor and O_2, CO, H_2S, NO_2, H_2, ethanol, and ammonia [17–22]. Therefore, the study of nano sensor devices based on TiO_2 with a stable environment and excellent performance has become an important research direction [23].

In this work, mesoporous TiO_2 precursors were synthesized by the biomimetic method under mild conditions using inexpensive raw materials and yeast cells as templates. The precursors were calcined at different temperatures (300–600 °C) for an hour and used as electrocatalytic materials to assemble the electrochemical sensing electrodes for the detection of pancreatic cancer miRNAs.

2. Experimental

2.1. Synthesis of yeast-templated TiO_2

A calculated amount of yeast cells was added to 30 mL of dextrose in water and incubated at ambient temperature. A uniform biological emulsion was formed after magnetic stirring for 30 min. The critical micelle concentration (CMC) of the bio-emulsion was *ca.* 6.7 mg mL^{-1}. A solution containing 10 mL of $TiCl_4$ (≥99.0%) and 20 mL of HCl (36–38%) was added into the above bio-emulsion in a dropwise fashion and under stirring for 24 h. An ammonia solution (25–28%) was then added dropwise to adjust the pH to 9–10. The resultant white precipitate was collected by centrifugation, carefully washed with distilled water and absolute ethanol, and dried at 80 °C in air. The obtained samples were heat-treated at different temperatures (300–600 °C) for 1 h to obtain the final products, which were denoted as YT_x ($x = 300$, 400, 500, and 600). All reagents were of analytical reagent grade.

2.2. Structure characterization

X-ray diffraction (XRD) measurements were performed at a PANalytical X'Pert PRO X-ray diffractometer with Cu K_α ($\lambda = 0.15418$ nm) incident radiation. The diffraction patterns were collected in the 2θ range of 10–70° (Cu K_α) at room temperature.

Nitrogen adsorption-desorption isotherms were acquired at 77 K using a computer-controlled sorption analyzer (Micromeritics, Gemini V2.0) operating in the continuous mode. The sample was degassed at 200 °C for 10 h before measurements. The pore size distribution was calculated from the desorption branch of the isotherm by the Barret-Joyner-Halenda (BJH) model.

Atomic force microscopy (AFM) measurements were carried out to examine the morphologies of the YT_x samples. The samples for AFM measurements were prepared by dispersing the samples in ethanol and then dropcasting the suspension onto a freshly cleaved mica piece. The samples were air-dried before data acquisition.

Elemental analysis was performed using a Hitachi S2450 scanning electron microscope in combination with Shimadzu Corporation's EPMA1600 X-ray energy spectrometer (EPMA).

2.3. Electrochemistry

The YT_x obtained above, acetylene black, activated charcoal, and polytetrafluoroethylene (PTFE) suspension (60 wt% in H_2O) at the mass ratio of 4:1:2:2 were uniformly mixed and dispersed in excess of ethanol to produce a dough-like paste. The paste was rolled into a sheet of 0.3 mm in thickness. Another sheet containing only acetylene black and PTFE at the mass ratio of 1:1 was prepared in the same manner. These two sheets were then rolled together and pressed onto a piece of nickel foam, which was then heat-treated at 200 °C for 2 h, producing a 0.5 mm thick air electrode.

Electrochemical measurements were performed in a three-electrode configuration. A large-area Pt disk and a Hg/HgO/OH^- (35 wt%) electrodes were used as the counter electrode and reference electrode, respectively. The air electrode produced above (1 cm^2) was used as the working electrode. An aqueous potassium hydroxide solution (35 wt%) was used as the electrolyte in all experiments. The polarization curves were acquired at the sweep rate of 10 mV s^{-1} with a CHI 660C electrochemical workstation.

2.4. Electrochemical detection of cancer miRNA

2.4.1. Materials and preparation of hybridization solution

miRNA oligonucleotides (or cDNA) were synthesized and purified by TSINGKE (http://www.tsingke.net/shop/). Various target miRNA (miR-1290) and match probe (e.g., Probe-miR-1290) or the related mismatch probes were mixed in 0.2 mL 10 μM hybridization solution at 90 °C for 2 min. The volume ratio of target miRNA: probe was 1:1.

2.4.2. Preparation of TiO_2 modified electrodes and cancer miRNA electrochemical detection

A glassy carbon electrode (GCE, 3 mm in diameter) was polished with 0.05 mm Al_2O_3 suspensions until a mirror surface was obtained, and rinsed extensively with anhydrous ethanol and deionized water. The electrode was then electrochemically cleaned in 0.5 M H_2SO_4 by cycling potentials between +0.3 and + 1.8 V at 100 mV s^{-1} until a steady cyclic voltammogram was obtained. 3 μL of a Nafion adhesive (0.02 % wt) was dropcast onto the cleaned GCE surface, onto which 3 μL of an ethanolic suspension of yeast TiO_2 (0.5 mg mL^{-1}) was added in a dropwise fashion. After drying, the

resulting electrodes were denoted as YT_x/GCE (x = 300, 400, 500, and 600).

Electrochemical measurements were performed in a three-electrode configuration. The YT/GCE electrodes prepared above were used as the working electrode. A Pt foil acted as the auxiliary electrode. All potentials were referred to an Ag/AgCl/KCl saturated reference electrode. The 10 μM hybridization solutions were diluted to 0.9 μM as analyte solutions. Voltammetric data were acquired with a CHI 660C electrochemical workstation.

3. Results and discussion

3.1. Characterization of mesoporous TiO_2 structure and composition

Mesoporous TiO_2 was prepared by using yeast cells as templates at different calcination temperatures. The structures were first characterized by XRD measurements. As illustrated in Fig. 1a, the sample prepared at 300 °C showed only amorphous diffraction patterns within the 2θ range of 20–30°, whereas the samples treated at higher temperatures (400–600 °C) showed a series of diffraction peaks that were consistent with those of anatase TiO_2 (JCPDS card number: 17–1167), 25.1° (101), 37.8° (004), 47.9° (200), 54.4° (105), 62.5° (204) [24]. Additionally, one can see that at increasing thermal annealing temperature, the diffraction peaks became sharper, suggesting enhanced crystallinity and crystallite sizes of the samples.

Interestingly, the resulting samples exhibited mesoporosity, as manifested in nitrogen adsorption-desorption isotherm measurements. From Fig. 1b, one can see that the nitrogen adsorption increases rapidly with the relative pressure P/P_0 in the range of 0.4–0.6. The adsorption and desorption processes become irreversible, and capillary condensation occurs. A distinct hysteresis loop appears in the isotherm, exhibiting typical mesoporous characteristics. Additionally, with increasing calcination temperature, the hysteresis loop evolved to a high relative pressure, indicating an increase of the pore size, likely because of further removal of the yeast templates. In fact, BJH analysis showed that the samples all possessed a rather narrow pore-size distribution and the main pore size increased from 3.8 to 4.7, 5.6, and 6.6 nm for the samples prepared at 300, 400, 500, and 600 °C, respectively (Fig. S1).

Fig. 2 shows the AFM images of the yeast-templated TiO_2 synthesized by calcination at 400 °C, which exhibits a highly ordered hierarchical wormhole-like texture and porous surface morphology.

Additionally, the samples also exhibited abundant oxygen vacancies. From the EPMA results in Table 1, one can see that the O/Ti ratio was over two at 300 °C, and no crystalline phase was formed at this calcination temperature, consistent with XRD results (Fig. 1a) where only amorphous phase was identified. By contrast, at higher calcination temperatures (400–600 °C), the O/Ti atomic ratios were all below 2, indicating the formation of oxygen vacancies in the samples, which reached the maximum for the sample prepared at 400 °C.

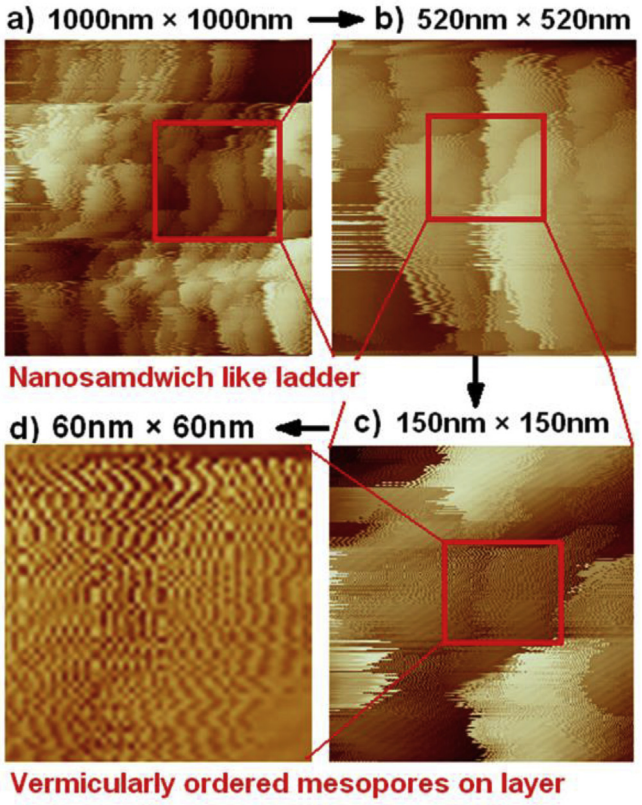

Fig. 2. AFM images of the yeast-templated TiO_2 synthesized by calcination at 400 °C at different length scales: (a) 1000 nm × 1000 nm, (b) 520 nm × 520 nm, (c) 150 nm × 150 nm, and (d) 60 nm × 60 nm.

Table 1
EPMA analysis for yeast-templated mesoporous TiO_2 prepared under different calcining temperatures.

	300 °C	400 °C	500 °C	600 °C
O: Ti	2.145	1.768	1.780	1.902
Phase	amorphous	β	β	α

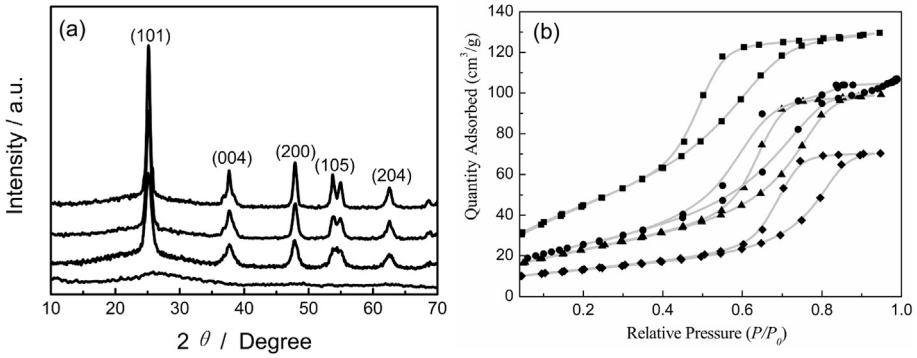

Fig. 1. (a) XRD patterns and (b) nitrogen adsorption-desorption isotherms for yeast-templated TiO_2 prepared at different calcination temperatures: 300 °C (■), 400 °C (●), 500 °C (▲), 600 °C (◆).

The electrocatalytic activity of the yeast-templated mesoporous TiO_2 towards oxygen reduction was then studied and compared. Fig. 3 shows the polarization curves of oxygen reduction at the various TiO_2 electrodes. One can see that within the potential range of 0 to −0.6 V, the sample prepared at 400 °C exhibited the highest voltammetric currents, indicating the best electrocatalytic activity towards oxygen reduction reaction among the series. For instance, the electrode potential needed to reach the current density of −40 mA cm^{-2} increases in the order of 400 °C < 600 °C ≈ 500 °C < 300 °C.

Notably, the electrochemical sensing progress in aqueous solution often involves oxygen reduction reaction shown in Eq. (1) − (3) [25], which can form HO_2^-, H_2O_2, and O_2^-. These peroxides (superoxides) formed in the aqueous solution facilitate the electro-oxidation of organic molecules including nucleic acid molecules [11], which can be exploited for electrochemical sensing. This is confirmed by subsequent electrochemical detection studies of pancreatic cancer miRNA.

$$O_2 + H_2O + 2e- \rightarrow HO_2^{-\cdot} + OH^- \quad (1)$$

$$O_2 + 2H_2O + 2e- \rightarrow H_2O_2 + 2OH^- \quad (2)$$

$$O_2 + e^- \rightarrow O_2^{-\cdot} \quad (3)$$

3.2. Electrochemical detection of pancreatic cancer miRNA

Pancreatic cancer is a relatively common malignant tumor with a very high degree of malignancy. miR-1290 is a specific marker of pancreatic cancer. Herein, we use the mesoporous TiO_2 sensing electrode to detect the perfect match and mismatch solutions for pancreatic cancer. Table 2 lists the target probe fragment sequences and their perfect match and mismatch fragment sequences. Under experimental conditions, the sensitivity of the YTs/GCE electrode to miR-1290 detection was 63.8 nA per μmolL-1 concentration (Fig. S2, see ESI† for details). Fig. 4 (left) shows the results of detection of pancreatic cancer miRNAs perfect match and mismatch solutions using a YT_{400}/GCE electrode. One can see that there is an oxidation peak at +0.2 V in curve a corresponding to the electro-oxidation of perfect match miR-1290, which is absent in all mismatch solutions, indicating that the YT_{400}/GCE electrode can selectively detect pancreatic cancer miRNA.

The right panel of Fig. 4 shows the SWV curves acquired with the perfect match solution of pancreatic cancer miR-1290 with unmodified GCE and YT_x/GCE electrodes. One can see that the anodic peak at 0.224 V appears only with the YT_x/GCE electrodes, but absent with the unmodified GCE, and the voltammetric peak current was the highest with YT_{400}/GCE. This suggests that the YT_{400}/GCE electrode exhibited the greatest sensitivity to miR-1290, among the series, coincident with its high electrocatalytic activity towards oxygen reduction reaction (Fig. 3).

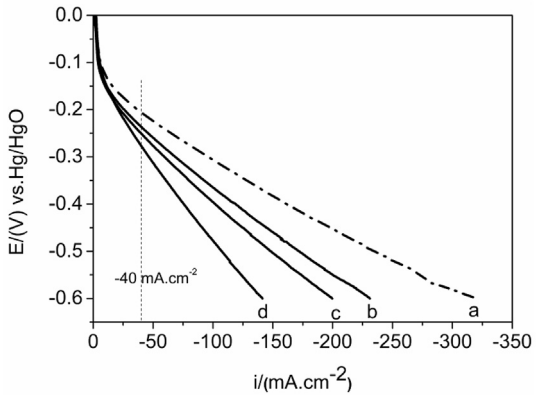

Fig. 3. Polarization curves for O_2 reduction with gas diffusion electrode loaded with bio-templated mesoporous TiO_2 obtained under different calcination temperature: (a) 400 °C; (b) 600 °C; (c) 500 °C; (d) 300 °C (sweep rate 10 mV s^{-1}).

Table 2
Matching and mismatching sequences for pancreatic cancer miR-1290.

Name	Sequence
miR-1290	5′-TGGATTTTTGGATCAGGGA-3′
Match Probe	5′-TCCCTGATCCAAAAATCCA-3′
Mismatch Probes	5′-TCCCTGATCAAAAAATCCA-3′
	5′-TCCCTGATCGAAAAATCCA-3′
	5′-TCCCTGATCTAAAAATCCA-3′
	5′-TCGCTGATCCAAAAATCCA-3′
	5′-TCCCGGATCCAAAAATCCA-3′
	5′-TCCCTGATCCAAACATCCA-3′
	5′-TCCCTGATCCAAAAATACA-3′

Note: mismatching sequences underlined.

The oxidation potential of miR-1290 perfect match solution is about +1.53 V at the unmodified GCE in curve e of Fig. 4 (right). Compared with the unmodified GCE, the oxidation potential of miR-1290 perfect match solution shifted negatively by +1.53 V to +0.224V at the YT/GCE, indicating that the mesoporous TiO_2 has the catalytic activity toward the electro-oxidation of pancreatic cancer miRNA at a markedly lower potential. This allows for an easy detection and minimize the interference of the sensing electrode by the oxygen evolution reaction at high potentials. And compared with other materials (e.g. commercial P-25, TiO_2 nanobelts), yeast TiO_2 has better electrochemical detective performance (Fig. S3, see ESI† for details).

4. Discussion

The difference of the electrocatalytic activity of the YT_x samples for detection of miR-1290 can be explained from the crystal form, pore structure, and oxygen vacancy. Among the three crystalline forms of TiO_2 (i.e., brookite, anatase, and rutile), anatase TiO_2 exhibits a more massive distortion, more open crystal structure and higher symmetry [26,27], thus has a stronger ability to adsorb organic matter and oxygen; and the anatase phase can be changed to rutile at temperatures higher than about 600 °C. The XRD results in Fig. 1 shows that the YT_{300} sample is mostly amorphous. After 400 °C, the samples change to anatase phase. With the increase of temperature, the purity of anatase phase TiO_2 increases gradually. Thus, the electrocatalytic activity of the YT_{400} sample for detection of miR-1290 is the best.

In electrochemical reaction, both mass transfer and electron-transfer are important factors dictating the reaction rate. Because the oxygen solubility (about 10^{-4} mol/L) and diffusion coefficient (10^{-9} m^2/s) in the electrolyte solution is very small, improving the mass transfer of oxygen is important for improving the electrochemical performance of the air electrode. Fig. S1 shows the pore size distribution curves of the YT_x samples. It can be seen that the YT_{300} sample has the smallest pore size of only 3.8 nm, likely because the yeast templates were hardly removed at this temperature. For YT_{400}, two major pore diameters were identified at 4.7 nm and 11.0 nm. At higher temperatures, the pore size increased accordingly, 5.6 nm for YT_{500} and 6.6 nm for YT_{600}. Since the average pore diameter is proportional to the pore volume and inversely proportional to the specific surface area, YT_{400} has both a large pore size and a small pore size. Therefore, the YT_{400} modified electrode has the best result of miR-1290 detection.

This can be further enhanced by the oxygen vacancies. Oxygen vacancies refer to defects due to oxygen escaping from their crystal lattice. Oxygen vacancies facilitate the rapid transport of oxygen in

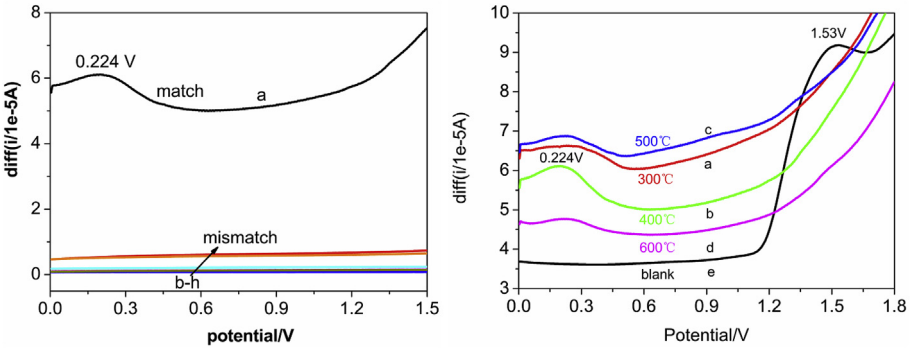

Fig. 4. (left) SWV curves for miRNAs match (a) and mismatch (b–h) at YT_{400}/GCE electrode. (right) SWV curves for the YT/GCE electrodes based on TiO_2 synthesized at different temperatures: (a) 300 °C, (b) 400 °C, (c) 500 °C, and (d) 600 °C. The control experiment with an unmodified GCE is shown in curve (e) (blank).

TiO_2 crystal lattice, which furtherly improve transport of peroxide (superoxide) intermediates and the electrochemical sensing performance. The EPMA results (Table 1) showed that the O/Ti ratio in the YT_x samples decreased first and then increased with the increase of calcination temperature, with YT_{400} showing the highest concentration of oxygen vacancies [28]. Therefore, YT_{400} has the best ability to electrocatalyze the oxidation of miR-1290.

5. Conclusions

In this work, using yeast cells as templates, mesoporous TiO_2 have been successfully prepared by calcination at 300–600 °C. The results of XRD, NADI, and EPMA show that the synthesized samples have different crystalline structures, pore size distribution, and oxygen vacancy, and hence different electrocatalytic activity towards oxygen reduction reaction. The results of electrochemistry indicate the obtained mesoporous TiO_2 can electrocatalyze the oxidation of the pancreatic cancer microRNAs and selectively detect a perfect match and mismatch pancreatic cancer miRNAs with single-nucleotide discrimination. Within the present experimental context, the sample prepared by calcination at 400 °C shows the best electrocatalytic activity and may serve as a promising active material for biosensor application of early cancer diagnosis and molecular biology research.

Declaration of competing interest

The authors declare that they have no known competing financial interests or personal relationships that could have appeared to influence the work reported in this paper.

CRediT authorship contribution statement

Xuping Wang: Writing - original draft, Formal analysis. **Jingjie Cui:** Writing - original draft. **Shaowei Chen:** Writing - original draft.

Acknowledgments

This research was supported by the Zhejiang Province Public Welfare Technology Application Research Project [LGF19E020002], Natural Science Foundation of Jiangsu Province [BK20181444], National Natural Science Foundation of China [51102152].

Appendix A. Supplementary data

Supplementary data to this article can be found online at https://doi.org/10.1016/j.aca.2020.01.030.

References

[1] World Health Organization, Early Cancer Diagnosis Saves Lives, Cuts Treatment Costs, 2017, pp. 2–3.
[2] F. Bray, J. Ferlay, I. Soerjomataram, et al., Global cancer statistics 2018: GLOBOCAN estimates of incidence and mortality worldwide for 36 cancers in 185 countries, CA-A Cancer J Clin 68 (2018) 394–424.
[3] Linda Rabeneck, Iris Lansdorp-Vogelaar, Best. Pract. Res. Cl. Ga. 29 (2015) 979–985.
[4] M. Scott, Hammond, Adv. Drug. Delivery. Rev. 87 (2015) 3–14.
[5] Mengying Cui, Xiaoxiao Yao, Lin Yang, Dan Zhang, Ranji Cui, Xuewen Zhang, J. Cell. Physiol. 18 (2019) 6–16.
[6] Zhichao Chen, Yiming Xie, Wan Huang, Chuanying Qin, Aimin Yua, Guosong Lai, Nanoscale 11 (2019) 11262–11269.
[7] Baraniskin Alexander, Stefanie Nöpel-Dünnebacke, Maike Ahrens, Steffen Grann Jensen, Hannah Zöllner, Abdelouahid Maghnouj, Alexandra Wos, Julia Mayerle, Johanna Munding, Dennis Kost, Anke Reinacher-Schick, Sven Liffers, Schroers Roland, Ansgar M. Chromik, Helmut E. Meyer, Int. J. Canc. 132 (2013) E48–E57.
[8] Ang Li, Jun Yu, Haeryoung Kim, Christopher L. Wolfgang, Marcia Irene Canto, Ralph H. Hruban, Michael Goggins, Clin. Canc. Res. 19 (2013) 3600–3610.
[9] Chunhong Zhu, Wanying Zhu, Lei Xu, Xuemin Zhou, Anal. Chim. Acta 1047 (2019) 21–27.
[10] Mariana C.O. Monteiro, Marc T.M. Koper, Electrochim. Acta 325 (2019) 134915.
[11] Xiaowei Chi, Yongan Tang, Xiangqun Zeng, Electrochim. Acta 216 (2016) 171–180.
[12] N. Sasikala, K. Ramya, K.S. Dhathathreyan, Energy Convers. Manag. 77 (2014) 545–549.
[13] Stefano Frangini, Silvera Scaccia, Int. J. Hydrogen Energy 39 (2014) 12266–12272.
[14] A.S. Groisman, N.E. Khomutov, Russ. Chem. Rev. 20 (1) (2010) 145–150.
[15] Liang-Bin Xiong, Jia-Lin Li, Bo Yang, Ying Yu, J. Nanomater. (2012) 1–13, 2012.
[16] Adel A. Ismail, Detlef W. Bahnemann, J. Mater. Chem. 21 (2011) 11686–11707.
[17] C. BuonoM, DesimoneF. SchipaniC, M. AldaoC, I. VignattiC, I.N. MorgadeG, F. CabezaT, F. Garetto, J. Electroceram. 40 (1) (2018) 72–77.
[18] Z.M. Seeley, A. Bandyopadhyay, S. Bose, Thin Solid Films 519 (1) (2010) 434–438.
[19] F.I.M. Ali, F. Awwad, Y.E. Greish, S.T. Mahmoud, IEEE Sensor. J. 19 (7) (2018) 2394–2407.
[20] M. Procek, A. Stolarczyk, T. Pustelny, E. Maciak, Sensors 15 (4) (2015) 9563–9581.
[21] B. Samransuksamer, T. Jutarosaga, M. Horprathum, A. Wisitsoraat, P. Eiamchai, S. Limwichean, V. Patthanasettakul, C. Chananonnawathorn, P. Chindaudom, Key Eng. Mater. 675–676 (2016) 277–280.
[22] Lü Renjiang, Wei Zhou, Keying Shi, Ying Yang, Lei Wang, Kai Pan, Chungui Tian, Zhiyu Ren, Honggang Fu, Nanoscale 5 (2013) 8569–8576.
[23] N. Phuong Khanh Quoc, K. Suzanne, Lunsford, Talanta. 101 (2012) 110–121.
[24] G. Zeng, K.K. Li, H.G. Yang, Y.H. Zhang, Vib. Spectrosc. 68 (2013) 279–284.
[25] N. Sasikala, K. Ramya, K.S. Dhathathreyan, Energy Convers. Manag. 77 (2014) 545–549.
[26] J. Yu, J. Low, W. Xiao, P. Zhou, M. Jaroniec, J. Am. Chem. Soc. 136 (25) (2014) 8839–8842.
[27] Ci Zhang Wen, Hai Bo Jiang, Shi Zhang Qiao, Hua Gui Yang, Gao Qing (Max) Lu, J. Mater. Chem. 21 (2011) 7052–7061.
[28] M. Setvin, U. Aschauer, P. Scheiber, Y.F. Li, W.Y. Hou, M. Schmid, A. Selloni, U. Diebold, Science 341 (6149) (2013) 988–991.